euronoise

A fast time-domain model for wheel/rail interaction demonstrated for the case of impact forces caused by wheel flats

Astrid Pieringer and Wolfgang Kropp

Chalmers University of Technology, Division of Applied Acoustics, SE-41296 Gothenburg, Sweden
astrid.pieringer@chalmers.se

The prediction of impact forces caused by wheel flats requires the application of time-domain models that are generally more computationally demanding than are frequency-domain models. In this paper, a fast time-domain model is presented to simulate the dynamic interaction between wheel and rail, taking into account the non-linear processes in the contact zone. Track and wheel are described as linear systems using impulse-response functions that can be precalculated. The contact zone is modelled by non-linear contact springs, allowing for loss of contact. This general model enables the calculation of the vertical contact forces generated by the small-scale roughness of rail and wheel, by parametric excitation on a discretely supported rail and by discrete irregularities of rail and wheel. Here, the model is applied to study the excitation caused by wheel flats by introducing a flat on a rotating wheel whose profile in the contact zone is updated in every time step. To demonstrate the functioning of the model, simulation results are compared to field measurements of impact forces and a brief parameter study is presented.

1 Introduction

A wheel flat is a defect of the running surface of a railway wheel, giving rise to noise and safety problems. This type of wheel damage occurs when the wheel locks and slides along the rail because of malfunction in the brakes or lack of wheel/rail adhesion due to e.g. snow or leaves on the rail. The sliding causes severe wear, leading to the wheel being flattened on one side. Subsequently, this out-of-round wheel generates large impact forces when it rotates. As a consequence, large vibration amplitudes of wheel and rail occur, resulting in high noise radiation. Furthermore, these impact forces may cause significant damage to the track or the wheel, causing for example the initiation and propagation of fatigue cracks [1].

The prediction of the dynamic interaction of railway wheel and track in response to discrete irregularities of the running surface such as wheel flats requires the application of time-domain models. In contrast to frequency-domain models, time-domain models are able to include a non-linear contact model. Non-linearities in the wheel/rail interaction cannot be neglected in the case of excitation by wheel flats because of the resulting large contact forces and the occurrence of loss of contact for train speeds above the critical speed [2, 3].

During the last 30 years, several time-domain models predicting the impact forces due to wheel flats have been published, e.g. [4–7]. In general, such time-domain models are computationally highly demanding. One possibility to reduce computational effort is to model wheel and rail using impulse-response functions (Green's functions) that can be precalculated and, by this means, to separate wheel, rail and contact calculations. This idea has already been successfully applied in the related area of tyre/road contact, see e.g. [8]. In the area of wheel/rail contact, the utilisation of Green's functions goes back to Heckl's proposal for a railway-simulation program [9]. Subsequently, this approach has been used by Nordborg [10] and recently by Mazilu [11].

The aim of this paper is to present a computationally efficient, but comprehensive time-domain model for dynamic wheel/rail interaction, which is able to simulate impact forces caused by wheel flats. For this purpose, the fast time-domain model earlier presented by Pieringer et al. in [12] is further developed and adapted to the excitation by wheel flats. Wheel and track are treated as linear and represented by Green's functions and moving Green's functions, respectively. The contact model is non-linear, comprising a bedding of independent springs (a Winkler bedding). This is an important difference compared to the above-mentioned models for wheel/rail interaction, which all - except [7] and [9] - include a single non-linear Hertzian contact spring between wheel and rail. Baeza et al. [7] compared the Hertzian model with a non-Hertzian model and concluded that the Hertzian model tends to overestimate the peak impact forces.

2 Modelling of wheel flats

Two kinds of wheel flat geometries are considered in this paper: the newly formed wheel flat with sharp edges as occurring right after formation and the rounded wheel flat, which rapidly develops from the newly formed flat as a result of wheel tread wear and plastic deformation.

The idealised newly formed wheel flat can be modelled as a chord of the wheel circumference, see Fig.1. Its length, l_0, its depth, d, and its centre angle, Φ_0, are related by

$$\frac{\Phi_0}{2} = \arcsin\left(\frac{l_0}{2R}\right) = \arccos\left(1 - \frac{d}{R}\right), \qquad (1)$$

with R being the wheel radius.

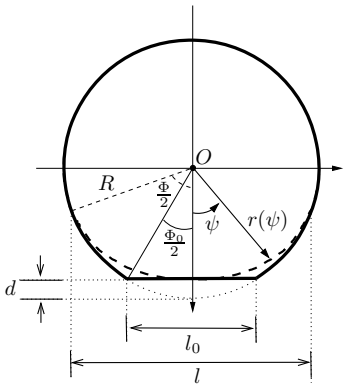

Figure 1: Geometry of newly formed and rounded wheel flat.

In the case of the newly formed flat, the wheel contour as function of the angle ψ is described by

$$r(\psi) = \begin{cases} \frac{R\cos\frac{\Phi_0}{2}}{\cos\psi} & \text{if} \quad \psi \in \mathrm{I}_{01} \\ R & \text{if} \quad \psi \in \mathrm{I}_{02} \end{cases}, \qquad (2)$$

where

$$\mathrm{I}_{01} = \left[0, 2\pi\right[\setminus \left[\frac{\Phi_0}{2}, 2\pi - \frac{\Phi_0}{2}\right] \qquad (3)$$

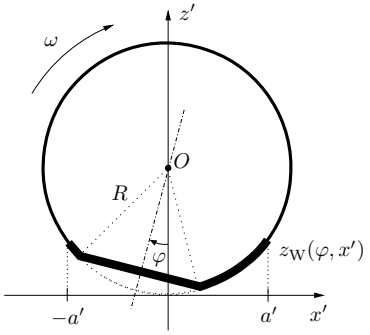

Figure 2: Newly formed wheel flat in angular position $\varphi > 0$.

$$\mathrm{I}_{02} = \left[\frac{\Phi_0}{2}, 2\pi - \frac{\Phi_0}{2}\right]. \quad (4)$$

The rounded flat is assumed to have the same depth, d, as the newly formed flat, but a length $l > l_0$. The centre angle, Φ, is obtained as before from the length

$$\frac{\Phi}{2} = \arcsin\left(\frac{l}{2R}\right). \quad (5)$$

Similar to the approach in [7], it is assumed that the contour $r(\psi)$ of the wheel with a rounded flat can be modelled by the function

$$r(\psi) = \begin{cases} R - \frac{d}{2}\left(1 + \cos\left(\frac{2\pi\psi}{\Phi}\right)\right) & \text{if} \quad \psi \in \mathrm{I}_1 \\ R & \text{if} \quad \psi \in \mathrm{I}_2 \end{cases}, \quad (6)$$

where

$$\mathrm{I}_1 = \left[0, 2\pi\right[\setminus \left[\frac{\Phi}{2}, 2\pi - \frac{\Phi}{2}\right] \quad (7)$$

$$\mathrm{I}_2 = \left[\frac{\Phi}{2}, 2\pi - \frac{\Phi}{2}\right]. \quad (8)$$

The contact algorithm requires the wheel profile expressed in Cartesian coordinates in the wheel-following coordinate system (x', z'). The orientation of the wheel in the wheel-following coordinate system (x', z') is described by the angle φ, $0 \le \varphi < 2\pi$, see Fig.2. For each φ, one obtains the profile $z_{\mathrm{W}}(\varphi, x')$ in the interval $[-a', a']$ as

$$\begin{pmatrix} x' \\ z_{\mathrm{W}}(\varphi, x') \end{pmatrix} = \mathbf{D}(\varphi) \begin{pmatrix} r(\psi^*)\cos\psi^* \\ r(\psi^*)\sin\psi^* \end{pmatrix} + \mathbf{T}, \quad (9)$$

where

$$\mathbf{D}(\varphi) = \begin{pmatrix} \cos\left(\varphi + \frac{\pi}{2}\right) & \sin\left(\varphi + \frac{\pi}{2}\right) \\ -\sin\left(\varphi + \frac{\pi}{2}\right) & \cos\left(\varphi + \frac{\pi}{2}\right) \end{pmatrix} \quad (10)$$

$$\mathbf{T} = \begin{pmatrix} 0 \\ R \end{pmatrix} \quad (11)$$

and

$$\psi^* \in \begin{cases} [\varepsilon_1, \varepsilon_2] & \text{if} \quad \varepsilon_1 \ge 0 \wedge \varepsilon_2 < 2\pi \\ [0, 2\pi[\setminus]\varepsilon_2, 2\pi + \varepsilon_1[& \text{if} \quad \varepsilon_1 < 0 \\ [0, 2\pi[\setminus]\varepsilon_2 - 2\pi, \varepsilon_1[& \text{if} \quad \varepsilon_2 \ge 2\pi \end{cases} \quad (12)$$

with

$$\varepsilon_1 = \varphi - \arcsin\frac{a'}{R} \quad (13)$$

$$\varepsilon_2 = \varphi + \arcsin\frac{a'}{R}. \quad (14)$$

The interval $[-a', a']$ has to be chosen as long enough to include all potential points of contact between wheel and rail (see section 3). The wheel profile as a function of the translational position, x, of the wheel centre writes as

$$z_{\mathrm{W}}(x, x') = z_{\mathrm{W}}(\varphi(x), x') = z_{\mathrm{W}}\left(\frac{x}{R} - 2\pi N_{\mathrm{r}}, x'\right), \quad (15)$$

where N_{r} is the number of accomplished wheel revolutions and the initial angular position of the wheel is assumed to be $\varphi(0) = 0$ for simplicity.

3 Wheel/rail interaction model

The wheel/rail interaction model presented schematically in Fig.3 is a moving vehicle model with constant train speed v.

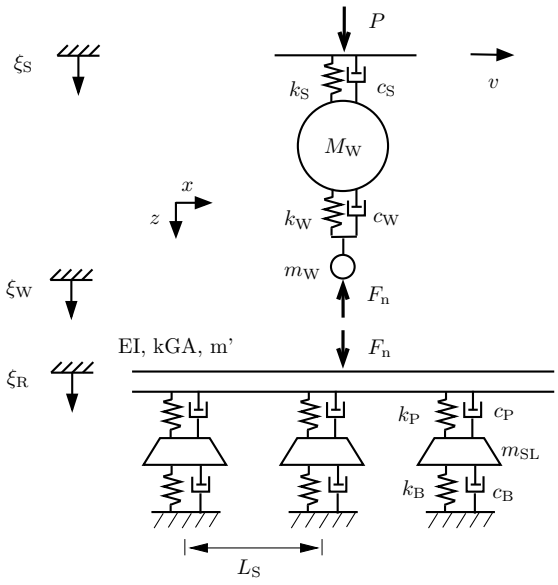

Figure 3: Wheel/rail interaction model.

3.1 Wheel and track model

The wheel model is a two-degree-of-freedom system (see Fig.3) with the parameters $M_{\mathrm{W}} = 592.5\,\mathrm{kg}$, m_{W}=3 kg, $k_{\mathrm{S}} = 1.12\,\mathrm{MN/m}$, $c_{\mathrm{S}} = 13.2\,\mathrm{kNs/m}$, $k_{\mathrm{W}} = 2.4\,\mathrm{GN/m}$ and $c_{\mathrm{W}} = 155\,\mathrm{kNs/m}$. This type of wheel model has shown good performance in previous studies [6, 13]. The wheel with radius $R = 0.45\,\mathrm{m}$ is represented in the time domain by its Green's function $\tilde{g}_{\mathrm{W}}(t)$, see Fig.4(a). The vehicle system above the primary suspension of the wheel is simplified to a static preload, P.

The track model is a linear finite element model accounting for discrete supports [5]. The UIC60 rail is modelled by undamped Rayleigh-Timoshenko beam elements with bending stiffness $EI = 6.4\,\mathrm{MNm^2}$, shear stiffness $kGA = 250\,\mathrm{MN}$ and mass per unit beam length $m' = 60\,\mathrm{kg/m}$. The length of the track model is 70 sleeper bays with sleeper spacing $L_{\mathrm{S}} = 0.65\,\mathrm{m}$. The discrete supports consist of railpads and sleepers on ballast (Fig.3) with pad stiffness $k_{\mathrm{P}} = 120\,\mathrm{MN/m}$ and damping $c_{\mathrm{P}} = 16\,\mathrm{kNs/m}$, (half) sleeper mass $m_{\mathrm{SL}} = 125\,\mathrm{kg}$ and ballast stiffness $k_{\mathrm{B}} = 140\,\mathrm{MN/m}$ and damping $c_{\mathrm{B}} =$

165 kNs/m. In the wheel/rail interaction model, the discretely supported rail is represented by moving Green's functions, $\tilde{g}^{x_0}_{\mathrm{R},v}(t)$ [12]. For excitation of the rail (index R) at the position x_0 at time $t_0 = 0$, the function $\tilde{g}^{x_0}_{\mathrm{R},v}(t)$ describes the displacement response of the rail at a point moving at train speed v away from the excitation, thus at the nominal contact point between wheel and rail. Three examples of moving Green's functions are shown in Fig.4(b).

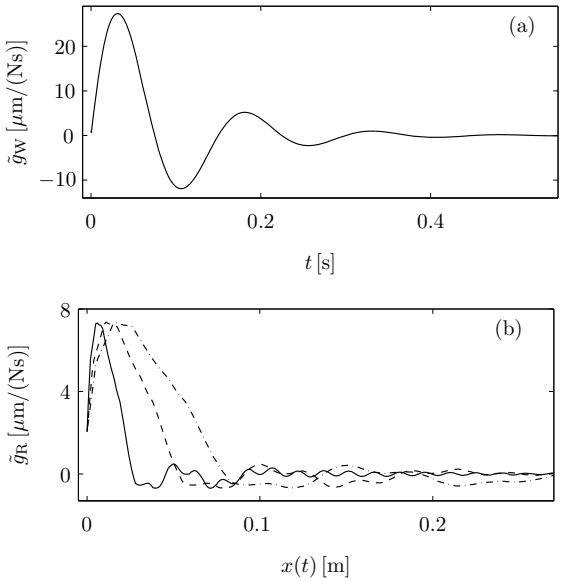

Figure 4: Green's function of the wheel (a). Moving Green's functions of the track for excitation at midspan between two sleeper positions (b) : —— $v = 50\,\mathrm{km/h}$, − − − $v = 100\,\mathrm{km/h}$, −·− $v = 150\,\mathrm{km/h}$.

3.2 Normal contact model

For the calculation of the normal contact force, F_n, a Winkler bedding is introduced between wheel and rail (see Fig.5). The springs in the bedding are independent and allow for loss of contact. The complete contact model is described by the following set of equations [12]

$$\xi_{\mathrm{S}} = \xi_{\mathrm{S}}(P) \tag{16}$$

$$\xi_{\mathrm{W}}(t) = -\int_0^t F_{\mathrm{n}}(\tau)\tilde{g}_{\mathrm{W}}(t-\tau)\,\mathrm{d}\tau + \xi_{\mathrm{S}}(P) \tag{17}$$

$$\xi_{\mathrm{R}}(t) = \int_0^t F_{\mathrm{n}}(\tau)\tilde{g}^{v\tau}_{\mathrm{R},v}(t-\tau)\,\mathrm{d}\tau \tag{18}$$

$$\Delta\zeta(x,x') = \xi_{\mathrm{W}}(x) - \xi_{\mathrm{R}}(x) + r(x+x') - z_{\mathrm{W}}(x,x') \tag{19}$$

$$F_{\mathrm{n}}(x) = \int_{-a'}^{a'} k(x,x')\,\Delta\zeta(x,x')\,\mathrm{d}x \tag{20}$$

$$k(x,x') = \begin{cases} \frac{1}{2}\frac{E}{(1-\nu^2)} & \text{if} \quad \Delta\zeta(x,x') \geq 0 \\ 0 & \text{if} \quad \Delta\zeta(x,x') < 0 \end{cases} \tag{21}$$

$$x = vt\,, \tag{22}$$

where ξ_{S} is the vertical position of the primary suspension and ξ_{W} and ξ_{R} denote the vertical position of the nominal contact point (at $x' = 0$) on wheel and rail, respectively. Furthermore, $\Delta\zeta$ is the contact-spring deflection, k the contact-spring stiffness, E the Young's modulus and ν the Poisson's ratio of wheel and rail (assumed equal for wheel and rail) and r is the combined roughness of rail and wheel being positive for an asperity on the rail.

In order to achieve that the bedding correctly models Hertz contact for smooth surfaces it is necessary to reduce the wheel radius to $R^* = 0.5\,R$ [14]. This implies that it is not possible to map the wheel flat geometrically correct on the reduced wheel. Theoretically, different modelling alternatives are possible. A previous experimental study of rounded wheel flats summarised by Johansson and Nielsen in [15] showed that the wheel-flat depth considerably influences the peak impact-force while the influence of the wheel-flat length is low. For this reason, it is chosen to keep the correct depth $d^* = d$ of the wheel flat on the reduced wheel and allow a length $l^* < l$.

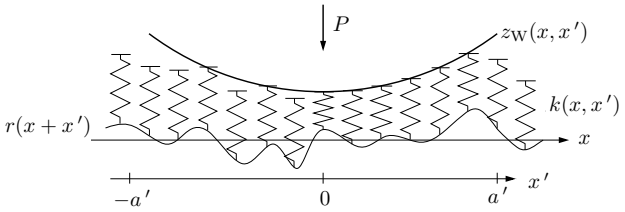

Figure 5: Bedding model for the wheel/rail contact.

4 Simulation results

4.1 Comparison to field measurements

To demonstrate the functioning of the modelling approach, simulation results are compared with field measurements from reference [15] in terms of the maximum impact load, see Fig.6.

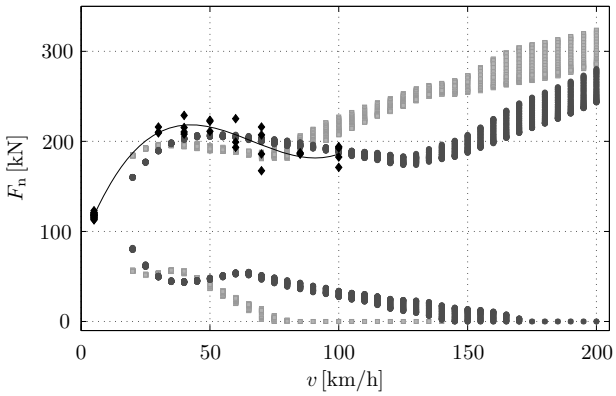

Figure 6: Measured maximum impact forces (⋄, black) due to a 0.9 mm deep rounded wheel flat in comparison to calculated maximum and minimum impact forces (○, dark grey). Shown are also a third-degree polynomial fitted to the measured data (——) and calculated results for a 0.9 mm deep new wheel flat (□, light grey).

In the field test, the impact load caused by a rounded wheel flat with depth $d = 0.9\,\mathrm{mm}$ and length $l = 0.1\,\mathrm{m}$ on a freight train with axle load 24 t ($P = 117.7\,\mathrm{kN}$) was measured for train speeds between 30 km/h and 100 km/h. As the receptance of the loaded track in the

frequency range of interest could not be measured during the field tests, Nielsen et al. determined rail pad and ballast parameters through model calibration [16]. These model parameters (listed in section 3.1) are also used in the present simulations. The small-scale roughness, r, of rail and wheel is set to zero. As the calculated impact force varies depending on where the wheel flat hits the rail in relation to the sleeper location, simulations with 40 different initial angular wheel positions, $\varphi(0)$, are run in order to cover the whole range of maximum impact-force magnitudes. Considering the uncertainty in the track parameters, the level of agreement between simulations and measurements seen in Fig.6 is encouraging.

4.2 Parameter study

Since a calculation with the presented wheel/rail interaction model takes typically only about one minute (on a PC with a Pentium 2.0 GHz processor), a parameter study including many simulations can be readily performed. The parameters investigated here are the train speed, the wheel flat depth and the type of wheel flat (new or rounded).

Fig.6 shows calculated maximum and minimum impact forces for train speeds from 20 km/h to 200 km/h. Beside the 0.9 mm deep rounded wheel flat, also a 0.9 mm deep new wheel flat is considered. In the case of the rounded wheel flat, the curve showing the maximum impact force has a local maximum at 50 km/h and a local minimum at 130 km/h. Loss of contact occurs for the first time at 145 km/h. The new wheel flat causes higher maximum impact forces than the rounded wheel flat, except in the speed range from 35 km/h to 85 km/h. The curve showing the maximum impact force has a local maximum at 40 km/h and a local minimum at 70 km/h. Loss of contact occurs already at 75 km/h. As a general tendency, it is observed that the variation in the maximum impact force due to different impact positions increases with speed.

The wheel and rail displacement and the normal contact force corresponding to two selected data points from Fig.6 are presented in Fig.7 as function of the wheel centre position x. The position $x = 0$ coincidences with a sleeper position. The two cases selected are the simulations at 50 km/h and at 150 km/h with the rounded wheel flat where the angular wheel position $\varphi = 0$ occurs at $x = 0.2\,L_S$. When the wheel flat enters the contact zone, the rail rises and the wheel falls which leads to partial unloading at 50 km/h and to loss of contact at 150 km/h. After the wheel has passed the angular position $\varphi = 0$, the wheel continues downwards and forces the rail to move downwards, too. The contact force increases rapidly and reaches the peak values of 207 kN and 192 kN at 50 km/h and 150 km/h, respectively. At the higher speed, the duration of the wheel flat passage in the contact zone is shorter and the wheel having a relatively large inertia does not fall as far as at the lower speed. This explains the lower impact force at higher speed.

Fig.8 further illustrates what happens in the contact zone during the passage of the wheel flat. The force in each contact spring (located at x') is displayed as function of the wheel centre position x. It can be clearly seen how the contact length varies and how the contact zone migrates under the wheel centre located at x (respectively $x' = 0$). With the wheel flat entering the contact zone, the contact zone moves behind the wheel centre. When the wheel flat leaves the contact zone, the contact zone is located ahead of the wheel centre.

Fig.9 shows the maximum and minimum impact forces

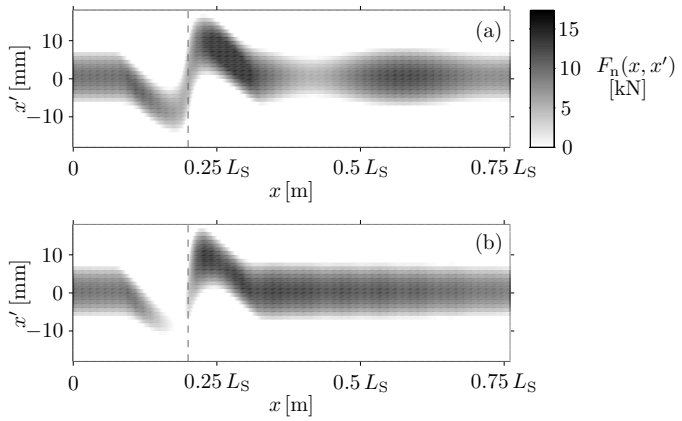

Figure 8: Longitudinal force distribution in the contact zone due to 0.9 mm rounded wheel flat as function of the wheel centre position x: (a) train speed 50 km/h. (b) train speed 150 km/h. The grey scale is the same for (a) and (b). The vertical lines indicate the position where $\varphi = 0$.

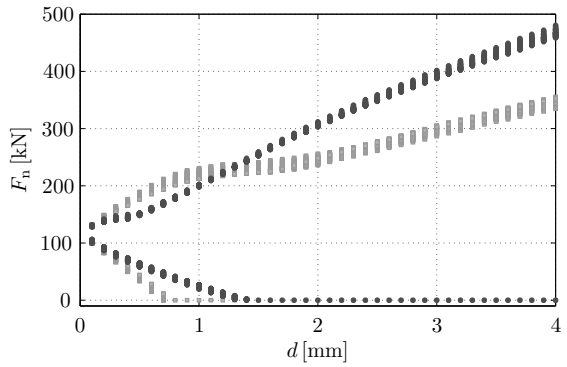

Figure 9: Maximum and minimum impact forces due to a rounded (○, dark grey) and a new (□, light grey) wheel flat at 100 km/h as function of the wheel flat depth.

for rounded and new wheel flats at 100 km/h with varying depths. The rounded wheel flats are assumed with the length $l = 1.76\,l_0$, l_0 being the length of the new wheel flat with the same depth. For both wheel-flat types, the maximum impact force increases with the depth. For small depths, the rounded wheel flat causes lower impact forces than the new wheel flat. For depths above 1.4 mm, the impact force due to the rounded wheel flat exceeds the one caused by the new wheel flat (Fig.9).

5 Conclusion

A numerical model has been presented, which simulates the wheel/rail interaction due to excitation by wheel

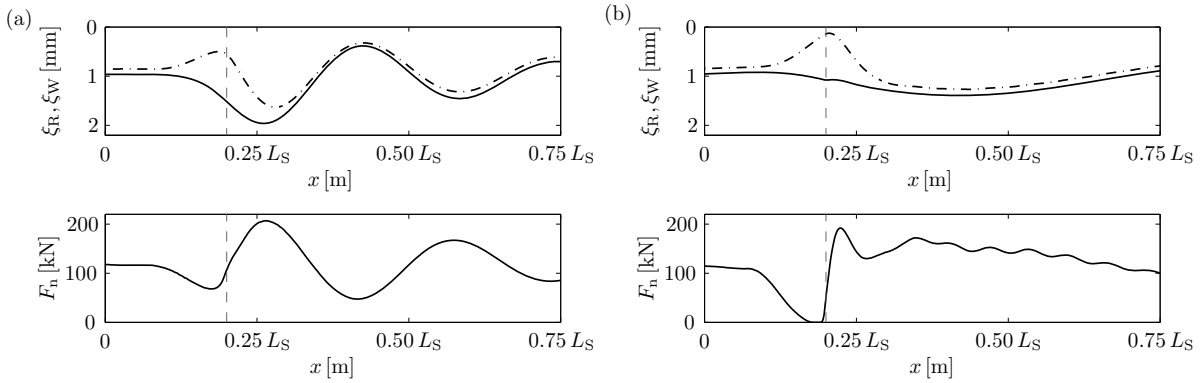

Figure 7: Displacement of wheel —— and rail $-\cdot-$ (upper) and normal contact force (lower) due to 0.9 mm rounded wheel flat: (a) train speed 50 km/h. (b) train speed 150 km/h. The vertical lines indicate the position where $\varphi = 0$.

flats. As wheel and rail are represented by precalculated Green's functions, the model is characterised by a high computational efficiency. Another advantage is that the model does not require to calculate an equivalent relative displacement excitation to represent the wheel flat. Instead, the actual wheel profile for each angular wheel position is included. A minor disadvantage of the model is however that length and depth of the wheel flat cannot be both at the same time mapped geometrically correct onto the reduced wheel required by the contact model. The encouraging level of agreement between measured and calculated impact forces demonstrates the functioning of the modelling approach.

6 Acknowledgements

The work described has been performed within the project "Generation of External Noise from Trains" (VB10) and forms part of the activities in the Centre of Excellence CHARMEC (CHAlmers Railway MEChanics). It is funded by CHARMEC in cooperation with VINNOVA, the Swedish Governmental Agency for Innovation Systems.

References

[1] J. Jergéus. Railway wheel flats - martensite formation, residual stresses, and crack propagation. PhD Thesis, Division of Solid Mechanics, Chalmers University of Technology, Göteborg, Sweden, 1998.

[2] D.J. Thompson and C.J.C. Jones. A review of the modelling of wheel/rail noise generation. *Journal of Sound and Vibration*, 231(3):519–536, 2000.

[3] I.L. Vér, C.S. Ventres, and M.M. Myles. Wheel/rail noise - Part III: Impact noise generation by wheel and rail discontinuities. *Journal of Sound and Vibration*, 46(3):395–417, 1976.

[4] S.G. Newton and R.A. Clark. An investigation into the dynamic effects on the track of wheelflats on railway vehicles. *Journal of Mechanical Engineering Science*, 21(4):287–297, 1979.

[5] J.C.O Nielsen and A. Igeland. Vertical dynamic interaction between train and track - influence of wheel and track imperfections. *Journal of Sound and Vibration*, 187(5):825–839, 1995.

[6] T.X. Wu and D.J. Thompson. A hybrid model for the noise generation due to railway wheel flats. *Journal of Sound and Vibration*, 251(1):115–139, 2002.

[7] L. Baeza, A. Roda, J. Carballeira, and E. Giner. Railway train-track dynamics for wheelflats with improved contact models. *Nonlinear Dynamics*, 45:385–397, 2006.

[8] F. Wullens and W. Kropp. A three dimensional contact model for tyre/road interaction in rolling conditions. *Acta Acustica united with Acustica*, 90(4):702–711, 2004.

[9] M. Heckl. Proposal for a railway simulation program. In *A Workshop on Rolling Noise Generation*, pages 128–148. Institut für Technische Akustik, Technische Universität Berlin, October 1989.

[10] A. Nordborg. Wheel/rail noise generation due to nonlinear effects and parametric excitation. *Journal of the Acoustical Society of America*, 111(4):1772–1781, April 2002.

[11] T. Mazilu. Green's functions for analysis of dynamic response of wheel/rail to vertical excitation. *Journal of Sound and Vibration*, 306:31–58, 2007.

[12] A. Pieringer, W. Kropp, and J.C.O. Nielsen. A time domain model for wheel/rail interaction aiming to include non-linear contact stiffness and tangential friction. In *Noise and Vibration Mitigation*, NNFM 99, pages 285–291. Springer-Verlag, Berlin Heidelberg, 2008.

[13] J.C.O Nielsen. High-frequency vertical wheel-rail contact forces - validation of a prediction model by field testing. In *Proceedings of the 7th International Conference on Contact Mechanics and Wear of Rail/Wheel Systems*, Brisbane, Australia, September 2006.

[14] R.A.J. Ford and D.J. Thompson. Simplified contact filters in wheel/rail noise prediction. *Journal of Sound and Vibration*, 293:807–818, 2006.

[15] A. Johansson and J.C.O. Nielsen. Out-of-round railway wheels - wheel-rail contact forces and track response derived from field tests and numerical simulations. *Proc IMechE Part F: Journal of Rail and Rapid Transport*, 217:135–146, 2003.

[16] J.C.O. Nielsen, J.W. Ringsberg, and L. Baeza. Influence of railway wheel flat impact on crack growth in rails. In *Proceedings of the 8th International Heavy Haul Conference*, pages 789–797, Rio de Janeiro, Brazil, 14-16 June 2005.